Fluid Phase Equilibria 346 (2013) 33–44

Contents lists available at SciVerse ScienceDirect

Fluid Phase Equilibria

journal homepage: www.elsevier.com/locate/fluid

Thermodynamic modeling of petroleum inclusions: Composition modeling and prediction of the trapping pressure of crude oils

Hongwei Ping[a,*], Honghan Chen[a], Régis Thiéry[b,c,d]

[a] Key Laboratory of Tectonics and Petroleum Resources (China University of Geosciences), Ministry of Education, Wuhan 430074, China
[b] Clermont Université, Université Blaise Pascal, Laboratoire Magmas et Volcans, BP 10448, F-63000 Clermont-Ferrand, France
[c] CNRS, UMR 6524, LMV, F-63038 Clermont-Ferrand, France
[d] IRD, R 163, F-63038 Clermont-Ferrand, France

ARTICLE INFO

Article history:
Received 9 December 2012
Received in revised form 5 February 2013
Accepted 6 February 2013
Available online 14 March 2013

Keywords:
Fluid inclusion
Trapping pressure
Saturation pressure
Thermodynamic modeling

ABSTRACT

Microthermometry and volumetric analysis have been widely used to reconstruct the composition and *P–T* trapping conditions of petroleum inclusions. However, a reliable prediction of the *P–T* trapping conditions requires efficient thermodynamic modeling of the *PVT* properties to obtain the saturation pressure and petroleum volume prediction in addition to accurate measurements of the homogenization temperature, T_h, and the degree of bubble filling, F_v. Until now, no critical appraisal of the volume prediction has been performed. Using an extensive compilation of data from the literature (909 points for the volume), we demonstrate that it is possible to have good predictions on the saturation pressures and volume characteristics of crude oils. Our improved F_v is correlated with the molar fraction of C_{7+} cut and the T_h value of the oil inclusion. We develop a new composition modeling method based on the α–β composition model by tuning the C_{7+} molar fraction. However, the ability of the new method to predict the trapping pressure is still strongly dependent on the accuracy of the saturation pressure estimation and the modeled F_v. A large number of reservoir fluids ($N = 160$) has therefore been used to derive the correlations between the trapping pressure prediction and the composition and saturation pressure. The formulation only relate to the molar fraction of methane. The new correlations are of interest as they reduce the number of relevant variables, in particular eliminating the effect of F_v on the trapping pressure prediction. Finally, we tested the accuracy of the new method in predicting the trapping pressure, emphasizing the influence of the bulk methane mole fraction on the trapping pressure. There is a need for future research on the prediction of the methane mole fraction in petroleum inclusions.

1. Introduction

Petroleum inclusions can supply important information regarding the trapping conditions, fluid compositions and post-trapping physical processes in petroleum-bearing sedimentary basins [1,2]. Reconstruction of the composition and *PVT* properties of trapped oil in individual fluid inclusions can be performed using petroleum inclusion thermodynamic modeling (*PITM*) with a specified homogenization temperature (T_h) and the degrees of bubble filling (F_v) in an α–β composition model or real fluid model [3–12], where the α–β model involves two adjustable parameters, α and β to approximate the full composition spectrum (C_1–C_{500}) of natural oils [5,13], and the "fluid model" uses postulated composition data [3,14], mainly, in the form of mole percentages for C_1, C_2, C_3, C_4, C_5, C_6 and C_{7+} and physical properties, *MW* and *SG*, respectively the molar weight and specific gravity of the C_{7+} cut. We review this method in Fig. 1. The first step is to measure T_h and F_v at room temperature (20 °C). Then, a composition model (α–β or fluid model) must be assumed to obtain the composition of the petroleum inclusion through an iterative calculation process [3,5] in which the oil composition is optimized to match the modeled T_h and F_v with their observed counterparts. Finally, the trapping conditions are calculated using the derived petroleum fluid composition and coeval aqueous fluid inclusion [3,5].

However, the *PITM* suffers from several problems. For example, the results based on the widespread method of Aplin et al. [3] depend strongly on the input composition of the petroleum inclusion chosen in the model [14]. Although the input composition can be selected based on a nearby reservoir, we cannot be confident that the input composition is close to that of the petroleum inclusion as many processes (e.g., oil cracking, gas de-asphalting, water washing and biodegradation) can drastically alter the composition of the inclusion following the petroleu maccumulation [15,16].

* Corresponding author at: Department of Petroleum Geology, Faculty of Resources, China University of Geosciences, Lumo Road No. 388, Hongshan District, Wuhan 430074, Hubei Province, China. Tel.: +86 27 67848512; fax: +86 27 67883051.
E-mail addresses: howping@yahoo.cn, howping@qq.com (H. Ping).

0378-3812/$ – see front matter.
http://dx.doi.org/10.1016/j.fluid.2013.02.016

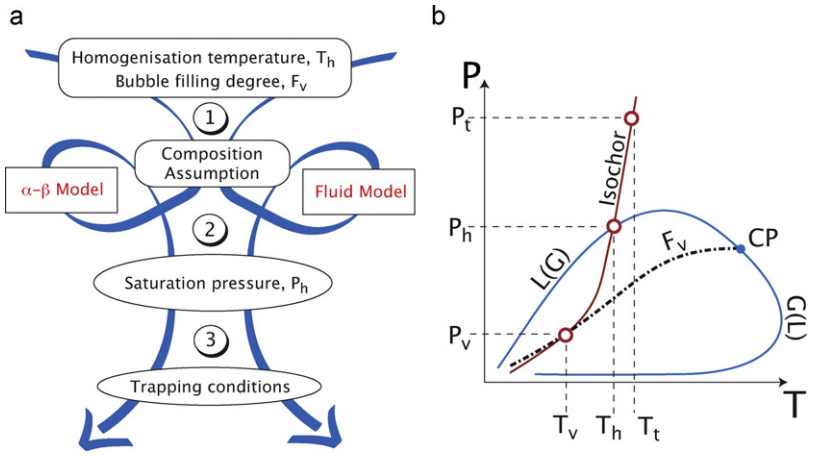

Fig. 1. (a) Schematic diagram of the steps in interpreting the microthermometric data. (b) Typical *P–T* phase diagram of a petroleum inclusion, illustrating the various elements required for the analysis of the microthermometric and volumetric data. The liquid–gas immiscibility loop is delimited by the bubble point (L(G)) curve and dew point (G(L)) curve, intersecting at the critical point (CP). The *P–T* path of the inclusion is described by an isochore with three points of interest: the (P_t, T_t) trapping point, the (P_h, T_h) homogenization point and the (P_v, T_v) point at which the degree of bubblefilling, F_v, is measured. The dashed-dotted curve is an isocurve of constant F_v.

Thiéry et al. [4,5] proposed a method using two parameters, α and β to describe the model composition of the natural petroleum. The advantage of this model is that it does not require the initial composition as input but rather utilizes the α–β composition model to fit the measured parameters (T_h and F_v) using thermodynamic calculations. However, the method of Thiéry, et al. suffers from the same composition uncertainty problem as that of Aplin et al. [3]; the α–β solution for T_h and F_v is a one-dimensional curve, $\beta(\alpha)$ (see Thiéry et al. [5] for further details).

Two types of parameters affect the results of the composition modeling and trapping condition calculations for petroleum inclusions. First, the input parameters, including measured values containing T_h and F_v or other optional parameters such as the gas oil ratio (*GOR*), American Petroleum Institute degree (*API*°) and C_1 mole content help to constrain the composition modeling. The T_h measurement is usually accurate to within ±0.1° and has been reported to estimate the volume of the cavity of an oil inclusion to an accuracy better than 95% [17]. The input parameters can therefore be determined with sufficient accuracy for the *PITM*. The second category of input parameter (the so-called thermodynamic parameters), which has a non-negligible impact on the accuracy of the *PVT* calculation, includes the parameters affecting the saturation pressure and volume predictions for the petroleum fluid, which in turn have a strong effect on the modeled F_v of the petroleum inclusion. The correlations used to determine the physical parameters of the petroleum cuts have been verified by the saturation pressure predictions of Ping et al. [12]. However, the determination of the trapping pressure (step 3 in Fig. 1) using *PITM* depends not only on the accuracy of the saturation pressure prediction [12] but also on the accuracy of the modeled F_v for the trapped composition calculated previously (steps 1–2 in Fig. 1) as the modeled fluid composition is determined by a match between the modeled T_h and F_v and their measured counterparts. The problem is whether the modeled F_v is accurate. To our knowledge, the prediction of F_v for petroleum inclusions has not been investigated in the literature, leading to the main question addressed in this paper: how can we confidently assess the precision of the F_v value used in the composition modeling of petroleum inclusions? How can we assess the accuracy of the trapping pressure prediction obtained using *PITM*? Ping et al. [12] have investigated the saturation pressure prediction of thermodynamic models of petroleum inclusions; however, the interpretation of the trapping pressure prediction is not straightforward, primarily owing to the lack of published data on the volume and trapping pressure of petroleum fluids. In the last decade, numerous *PVT* studies have been made publicly available (see e.g., [12,18,19] and references therein), which may shed new light on this problem.

It is clear that the saturation pressures and modeled F_v values of petroleum fluids are important affective parameters in the trapping pressure reconstruction with *PITM*. In this study, a method for calibrating the volume prediction for petroleum fluids is presented. Although a reliable calculation of the F_v value is possible, we will demonstrate that the modeled composition and trapping pressure are sensitive to the accuracy of the modeled F_v. Furthermore, we demonstrate that both the saturation pressure at T_h and the trapping pressure at trapping temperature T_t (which slightly exceeds T_h, e.g., $T_t = T_h + 5°$) are strongly related to the C_1 mole percent in petroleum fluids. Finally, we present an empirical formula for the trapping pressure prediction as a function of the C_1 molar content of the petroleum inclusion.

2. Calculation method

The accuracy of the saturation pressure calculation plays an important role in the volume prediction. The saturation pressure of oils should therefore be matched to the experimental value before volume calculation. The compositions of petroleum fluids are always expressed as weight fractions and the molecular weight measurement of the plus fraction typically has an experimental error of approximately ±(5–20%) [20–22], causing substantial variation in the molecular weight of the plus fraction, which is used as the primary tuning parameter. Only the molecular weight of the plus fraction is usually used as the tuning variable for matching saturation pressure with the extended composition [20–22]. However, we found that if the density of the plus fraction is adjusted simultaneously, then the variation of the *MW* and density of the plus fraction can be reduced significantly compared to those obtained by adjusting the *MW* of the plus fraction alone. In this study, the saturation pressure is therefore matched using the extended composition by adjusting both the *MW* and density of the plus fraction. The *MW* of the plus fraction is adjusted within the minimum experimental error to achievethe saturation pressure calculated. The detailed rationale underlying this approach is described in Appendix A.

Experimental volume data are used to calibrate the volumes in the gas and liquid phases, which are calculated using a volume translation based on the equation of state (*EOS*). The volume calibration method for petroleum fluids is provided in Appendix B.

The basic calculation scheme to match the experimental volume includes the following steps:

(1) Splitting the C_{7+} fraction into a number of pseudo-components based on their mole fractions, molecular weights (*MW*) and specific gravities (*SG*).
(2) Estimating the physico-chemical properties (the critical temperature T_c, critical pressure P_c, acentric factor ω, molecular weights *MW*, specific gravities *SG*, and normal boiling temperature T_b) of the pseudo-components using the appropriate correlations.
(3) Grouping the pseudo-components into a smaller set of pseudo-components. The properties of the new pseudo-components are computed from the old ones using mixing rules.
(4) Tuning the experimental *MW* and *SG* values of the heptane plus composition slightly to match the saturation pressure at a given temperature for the grouped composition (Appendix A). The experimental relative volume data are then matched using the adjusted composition (Appendix B).
(5) Using *PR-EOS* [23] to perform the *PVT* and phase equilibrium calculations.

The number of variants on this general calculation scheme is quite large, and we have chosen the following arbitrary options:

(1) The C_{7+} cut is split into a series of pseudo-components ranging from C_7 to C_{44} plus a final C_{45+} term using the algorithm described in [24]. The C_{45+} pseudo-component was chosen as the final component because the parameters for compounds with higher carbon numbers are not defined in some current methods (e.g., Katz and Firoozabadi [25]).
(2) Preliminary calculations have shown that the saturation pressure calculation results are sensitive to the choice of correlation used to calculate the pseudo-component parameters (T_c, P_c, T_b, ω) [12]. A number of correlations have been widely developed for computing the critical properties (T_c, P_c and T_b) and acentric factor (ω) of hydrocarbon [26–34]. In this study, we have therefore tested several correlations of them. Several combinations of correlations are possible, and we consider nine different calculation methods, which are listed in Table 1. The critical properties and accentric factor of each single carbon number (*SCN*) are well-documented for hydrocarbons with low carbon numbers (C_1–C_6) [35]. Some correlations express the critical properties in terms of the boiling temperature, T_b, and specific gravity, *SG*, rather than in terms of the laboratory observables (*MW* and *SG*). In this case, an additional equation is required to connect the *MW*, T_b and *SG* parameters. The *MW* and T_b values for each *SCN* group (C_7–C_{44}) are assigned using the tabular correlation provided by Katz and Firoozabadi [25]. The *MW* and T_b values of theC_{45+} component can be obtained using the methods of Ahmed et al. [24] and Pedersen et al. [36], respectively. We estimated the *SG* values of C_7–C_{45+} using the *MW* values and a correlation for the Watson characterization factor, *K*, which is assumed to be constant for a given fraction [37]. The *K* value can be obtained using the correlation of Zurita et al. [21].
(3) The pseudo-components are lumped into six groups: C_7, C_8, C_9, C_{10}, C_{n1} and C_{n2}. The C_{n1} group contains compounds with carbon atom numbers *n* between 11 and 25, andC_{n2} includes those components with *n* greater than or equal to 26. This grouping scheme is the same as that used in the α–β model [5]. The resulting components after grouping are N_2, CO_2, H_2S, C_1, C_2, C_3, *i*-C_4, *n*-C_4, *i*-C_5, *n*-C_5, C_6, C_7, C_8, C_9, C_{10}, C_{n1}, and C_{n2}. Kay's mixing rules [33,38] are applied to calculate the parameters (T_c, P_c, ω, *MW*, *SG*, T_b).
(4) The match to the saturation pressure of the oil follows the procedures described in Appendix A.
(5) The binary interactions parameters (BIPs) k_{ij} between the hydrocarbons can be estimated by a group contribution method [39,40], however, the objective is not to find the optimum BIPs that leads to accurate prediction of the saturation pressure, and so the BIPs between the hydrocarbon were set to zero for simplify; the interaction parameters were nonzero for the hydrocarbon to non-hydrocarbon interactions [21].

Table 1
Critical properties calculation of extended composition (C_7–C_{45+}) with different methods.

Method	Critical temperature and pressure (T_c and P_c)	Acentric factor (ω)
1	Cavett (1962)[a]	Riazi and Al-Sahhaf (1996)[b]
2	Cavett (1962)[a]	Edmister (1958)[c]
3	Winn (1957)[d]	Riazi and Al-Sahhaf (1996)[b]
4	Riazi and Al-Sahhaf (1996)[b]	Edmister (1958)[c]
5	Kesler-Lee (1976)[e]	Edmister (1958)[c]
6	Riazi-Daubert (1980)[f]	Riazi and Al-Sahhaf (1996)[b]
7	Kesler-Lee (1976)[e]	Riazi and Al-Sahhaf (1996)[b]
8	Twu (1984)[g]	Edmister (1958)[c]
9	Pedersen and Christensen (1989)[h]	Pedersen and Christensen (1989)[h]

[a] T_c and P_c were calculated using Cavett (1962) method [26].
[b] ω was calculated using Riazi and Al-Sahhaf (1996) method [27].
[c] ω was calculated using Edmister (1958) method [28].
[d] T_c and P_c were calculated using Winn (1957) method [29].
[e] T_c and P_c were calculated using Kesler-Lee (1976) method [30].
[f] T_c and P_c were calculated using Riazi-Daubert (1980) method [31].
[g] T_c and P_c were calculated using Twu (1984) method [32].
[h] T_c, P_c and ω were calculated using Pedersen and Christensen (1989) method [33].

3. Results and discussion

3.1. Correlation comparisons for the saturation pressure prediction

The 160 measurements of the saturation pressure and compositions of a variety of crude oils collected from the literature were used to match the modeled saturation pressure [19,38,41–61]. To check the accuracy of the various correlations, we compared the experimental and adjusted values of *MW*, *SG* and the composition. To measure the composition, we take the absolute mean deviation, Δx, of the molar fractions, x_i, of the various cuts (C_1, C_2, C_3, C_4, C_5, C_6, C_{7+}) as follows:

$$\Delta x = \frac{1}{7}\sum_{i=1}^{7+}\left|\frac{x_{i,tun} - x_{i,\exp}}{x_{i,\exp}}\right| \quad (1)$$

Next, the deviations of the experimental values from the adjusted values (*MW* and *SG*) are quantified using classical statistical parameters.

The average absolute deviation of *P*, *AAD* (*P*), is defined by:

$$AAD\ (P) = \frac{1}{N}\sum_{i=1}^{N}\left|\frac{P_{tun} - P_{\exp}}{P_{\exp}}\right|, \quad (2)$$

where *N* is the number of data points and *P* is either the *MW* or *SG* of the C_{7+} cut.

Similarly,

$$AAD(V) = \frac{1}{N}\sum_{i=1}^{N}\left|\frac{V_{cal} - V_{\exp}}{V_{\exp}}\right|. \quad (3)$$

Table 2
Variations in *MW* and *SG* for the heptane plus fraction using various methods to match the saturation pressures of the crude oils.

Method	*AAD* (*SG*)	*AAD* (*MW*)	*AAD* (*x*)	Validated
1	1.94	4.94	2.21	√
2	2.25	5.63	2.66	√
3	21.97	85.44	24.54	
4	9.14	30.24	10.53	
5	8.46	32.38	9.47	
6	2.55	7.25	2.91	√
7	2.88	9.28	3.36	√
8	27.55	119.47	31.22	
9	4.32	14.34	10.38	

Here V_{cal} is the calculated relative volume (V_t^{rel} or $V_t^{rel'}$) with or without volume calibration and V_{exp} is the experimental relative volume (V_t^{rel} and $V_t^{rel'}$).

Table 2 shows the variation in the *MW* and *SG* values of the heptane plus fraction required to match the saturation pressure using 9 different set of correlations (Table 1) to calculate the parameters (T_c, P_c, ω, *MW*, *SG*, T_b) of the extended composition. The criterion for selecting the critical property correlations is to minimize the required adjustment of the *MW* and density of the plus fraction to match the measured saturation pressure. The best results are obtained using methods (1), (2), (6), and (7). However, the set of correlations leading to the smallest adjustment in the *MW* and density of the heptane plus fraction is method (1), in agreement with the conclusions of Zurita et al. [21] and Al-Meshari [42]. In the remainder of the analysis, we employ method (1).

3.2. Volume calibration

The 909 relative volume data points (*N* = 397 (*CME*), *N* = 71 (*DV*), *N* = 441 (*SWT*)) collected from the literature [18,42,62] were used to match the calculated values by adjusting the coefficients *d* and *e* (Eq. (B.12)) in the *PR-EOS*. The regressed coefficients *d* and *e* for the volume shift parameters for pseudo-components C_{n1} and C_{n2} are 2.3 and 0.1, respectively. The accuracies of the method used in this paper (method 1) and the other eight methods (Table 1) for estimating the saturation pressures and relative volumes (V_t^{rel} and $V_t^{rel'}$) of various crude oils are listed in Table 3. It can be seen from Table 3 that methods 1 and 2 are the most accurate for the saturation pressure and relative volume calculations with no volume translation; methods 6, 7 and 9 are far superior to methods 3, 4, 5 and 8, which have large average deviations for both the saturation pressure and relative volume predictions. The accuracy of the relative volume calculation can be improved by employing the volume translation method. As shown in Table 3, the *AAD*% values of the calculated relative volume for *CME*, *DV* and *SWT* using method 1 are 0.83, 1.58 and 0.78, respectively, and the accuracy of the results is improved relative to those obtained without the volume translation. Overall, method 1 provides the most accurate volumetric prediction. Note

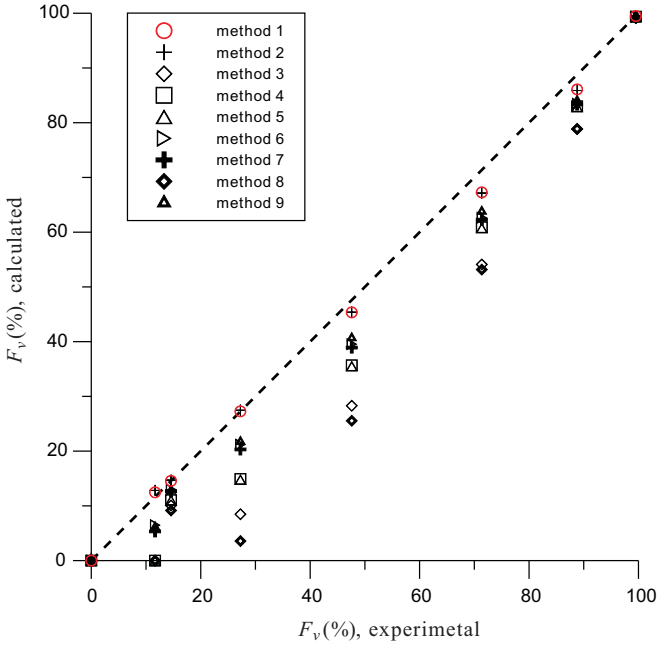

Fig. 2. Comparison of the experimental F_v of fluid F5 [18] with the values calculated by the methods in Table 1 using the volume calibration method.

that the proposed method provides a superior prediction primarily because of its accuracy in the saturation pressure prediction. A reliable volume prediction for petroleum fluid cannot be obtained without a reliable previous estimation of the saturation pressure.

One question remains. The relative volume estimate has been improved by the volume translation method. How accurately can the degree of bubble filling, F_v, be estimated using the proposed method? A definite answer to this question would require experimental data. However, no direct experimental F_v data have been published in the literature thus far. Nevertheless, an equivalent F_v can be obtained using Eq. (B.6) when both V_t^{rel} and $V_t^{rel'}$ are known under the same *P*–*T* conditions as the experimental data. In this paper, we use a dimensionless compressibility function, commonly known as the Y-function, to extrapolate V_t^{rel} to the *P*–*T* conditions under which $V_t^{rel'}$ is measured, and the Y-function is frequently used to smooth the values of the relative volume (V_t^{rel}). To smooth the relative volume data below the saturation pressure, the Y-function is plotted versus pressure on a Cartesian scale. The Y-function forms a straight line or has only a small curvature. It is therefore possible to recalculate the relative volume at all pressures below the saturation pressure. Figs. 2–4 display comparison diagrams between the calculated F_v and equivalent F_v from the experimental relative volume of fluid, F5, F12 and F13 [18]. Note that method 1 predicts F_v values that are in good agreement with the equivalent F_v values, whereas the other methods do not reproduce the equivalent

Table 3
Comparison of the various methods for calculating the relative volume of the crude oils.

Method	*AAD* (%), (P_s)	*AAD* (%), constant mass expansion (V_t^{rel})		*AAD* (%), differential vaporization ($V_t^{rel'}$)		*AAD* (%), isothermal swelling test (V_t^{rel})	
		Without volume calibration	Volume calibration	Without volume calibration	Volume calibration	Without volume calibration	Volume calibration
1	**0.09**	**1.50**	**0.83**	**2.81**	**1.58**	**0.90**	**0.78**
2	3.03	1.89	1.12	2.42	2.14	0.99	0.92
3	31.34	14.35	14.77	4.32	4.39	8.05	7.88
4	28.67	6.19	6.77	4.81	4.01	7.34	7.26
5	28.00	5.89	6.34	4.77	4.01	7.40	7.32
6	10.14	2.28	2.98	2.65	2.17	2.66	3.12
7	12.67	2.81	3.47	3.03	2.52	3.72	4.06
8	37.75	23.07	10.69	5.52	5.08	10.76	10.28
9	9.90	2.08	2.68	2.64	2.00	3.06	3.45

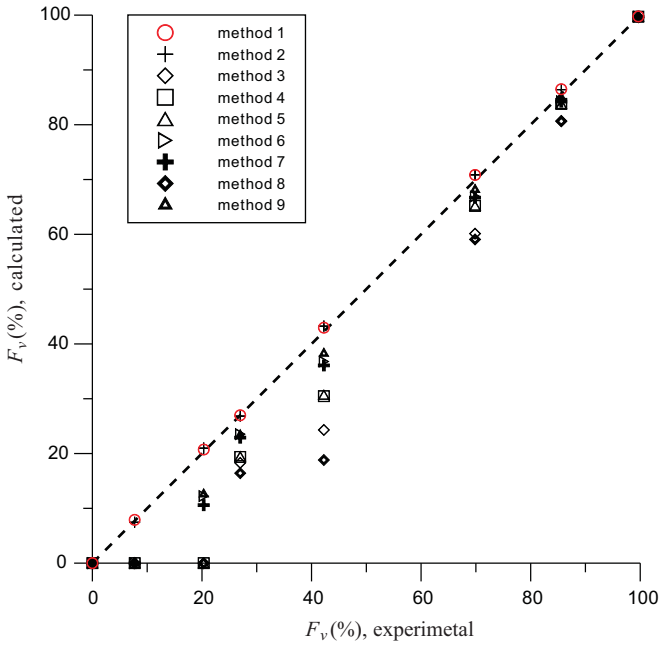

Fig. 3. Comparison of the experimental F_v of fluid F12 [18] with the values calculated by the methods in Table 1 using the volume calibration method.

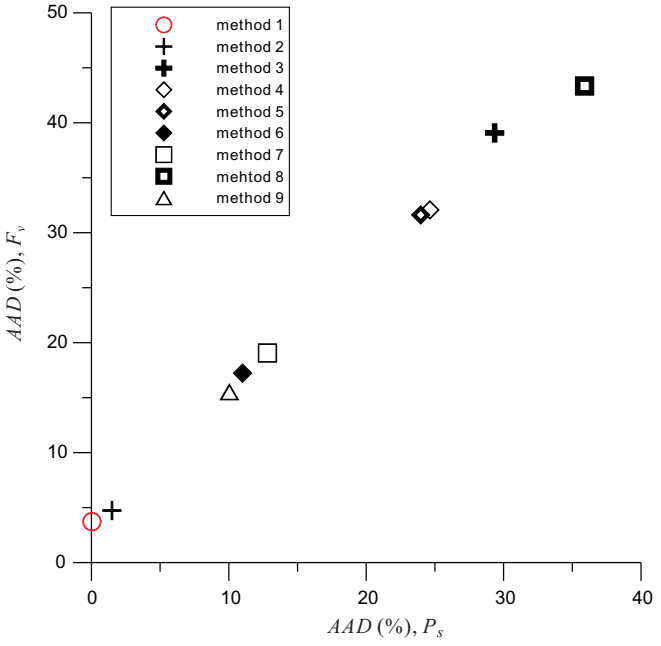

Fig. 5. Effect of the saturation pressure estimation on the accuracy of the calculated F_v using the methods in Table 1.

F_v values. The linear correlation between the AAD(%) of the F_v and saturation pressure predictions in Fig. 5 shows that the reason for the discrepancies in the F_v values predicted by the other methods is discrepant saturation pressure predictions. This observation is in accordance with the conclusion that the saturation pressure plays an important role in the volume prediction.

3.3. The effect of F_v on the composition modeling and saturation pressure prediction

The α–β model [4,5] has been used in petroleum inclusion thermodynamic modeling for more than ten years; however, the factors impacting the modeled results are not fully understood. Ping et al. [12] recently assessed the abilities of several fluid models (the α–β model, β model, and fluid model) to predict the saturation pressure. Note that the saturation pressure prediction for these models is based on the known fluid composition and physical properties (MW and SG) of the C_{7+} cut of the crude oils. For petroleum inclusions, the fluid composition should be determined by solving for the α–β value that yields the measured T_h and F_v. The uncertainty in the composition modeling, which affects the accuracy of the composition and saturation pressure predictions, therefore increases with the uncertainty in the modeled F_v. We next elaborate on this point through an example. For an inclusion with T_h = 54.41 °C and F_v = 3% measured at 20 °C, the α–β solutions are given by the black line (a) in Fig. 6. For comparison, we have calculated the α–β solutions for the inclusion under two conditions: a modeled F_v with a ±1% deviation compared to the given F_v (3%). The α–β solutions are given by the black lines b and c in Fig. 6. Note that the α–β solutions (the $\beta(\alpha)$ curve) for the same inclusion (T_h = 54.41 °C and F_v = 3%) are different for different prediction accuracies of F_v. For further comparison, we assumethat the inclusion (T_h = 54.41 °C, and F_v = 3%) has a 27.1% methane mole percent, whose α–β solution and calculated characteristics are given in Table 4. The corresponding α–β points are plotted in Fig. 6.

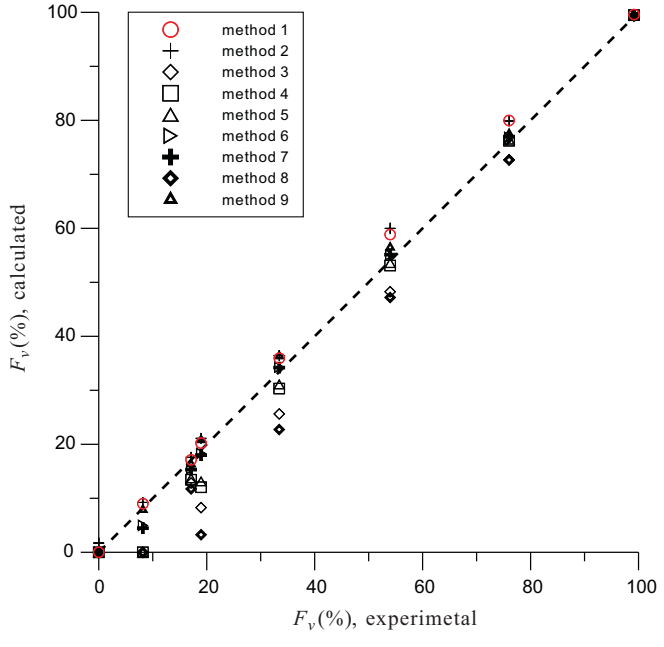

Fig. 4. Comparison of the experimental F_v of fluid F13 [18] with the values calculated by the methods in Table 1 using the volume calibration method.

Note that the three compositions calculated using the α–β model yield discrepant compositions and saturation pressures, especially for the plus fraction (C_{7+} and C_{n2}), where a maximum deviation of 10 mol% has been caused by the 1% deviation in the calculated F_v although the three compositions have similar saturation pressures. We next assume that the inclusion (T_h = 54.41 °C, and F_v = 3%) has a 41.7% methane mole percent, whose α–β solution and calculated characteristics are provided in Table 5. The corresponding α–β points are plotted in Fig. 6. Table 5 shows that the deviation of 1% in the calculated F_v can produce an absolute deviation (AD) of 25% in the saturation pressure prediction. The examples of Tables 5 and 6 demonstrate the importance of the volume prediction in composition modeling and pressure prediction for petroleum inclusions.

Table 4
Comparison of the estimation of the composition and saturation pressure with the α–β model for a petroleum inclusion with T_h = 54.4 °C, F_v = 3% at 20 °C and x_1 = 27.1% (In. 1); with the values estimated with the α–β model whose calculated F_v has a 1% negative deviation (In. 3); or a 1% positive deviation (In. 2).

Solution	α	β	P_h (MPa)	x_1 (mol%)	x_{7+} (mol%)	x_{n1} (mol%)	x_{n2} (mol%)
In. 1	0.9198	0.3980	8.90	27.1	48.3	22.4	9.0
In. 2	0.8822	0.3078	8.45	27.1	43.6	19.8	3.6
In. 3	0.9492	0.4840	9.74	27.1	53.4	21.8	18.4

Table 5
Comparison of the saturation pressure estimate with the α–β model for a petroleum inclusion with T_h = 54.4 °C, F_v = 3% at 20 °C and x_1 = 41.7% (In. 4); with the values estimated with the α–β model whose calculated F_v has a 1% negative deviation (In. 6); or a 1% positive deviation (In. 5).

Solution	α	β	P_h (MPa)	x_1 (mol%)	x_{7+} (mol%)	x_{n1} (mol%)	x_{n2} (mol%)
In. 4	0.9500	0.6130	18.56	41.7	38.1	15.5	13.3
In. 5	0.9326	0.5736	16.73	41.7	35.0	15.5	8.4
In. 6	0.9673	0.6706	23.08	41.7	42.0	13.6	21.0

3.4. A new correlation for α–β composition modeling

In the previous section, we have demonstrated that the calculated F_v value has a significant impact on the modeled composition and predicted saturation pressure. The α–β model cannot provide a reliable prediction of the F_v value of a petroleum inclusion unless a high-accuracy saturation pressure prediction and volume calibration have first been achieved. To our knowledge, no model is available that can provide accurate predictions of both the saturation pressure and volume properties.

Ping et al. [12] has proven that F_v (%) is correlated with T_h (°C) and theC_{7+} content (in mol%). In this study, a strong correlation is found between F_v and C_{7+} for different T_h values after matching the saturation pressure and volume calibration, as shown in Fig. 7. A mathematical relationship between T_h and the C_{7+} mole percentage has been obtained using multilinear regression (Eq. (4)). The standard deviation of the residuals between the fitted and calculated C_{7+} values is 2.37 mol% for the C_{7+} fraction:

$$C_{7+} = aF_v{}^b \times 100\% \quad (4)$$

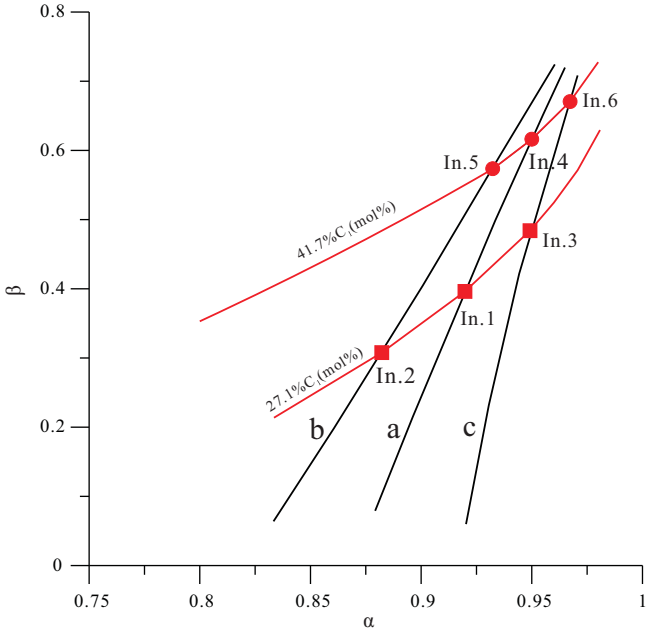

Fig. 6. Determination of the α–β solution. The red lines are isocurves of the C_1 mole percent. The black lines, a, b, and c, are examples of $\beta(\alpha)$ curves calculated for three petroleum inclusions (see the text for details). The six marks with the numbers 1, 2, 3, 4, 5, and 6 refer to the α–β fluid in Tables 5 and 6. (For interpretation of the references to color in this figure legend, the reader is referred to the web version of this article.)

where a and b are the coefficients given as a function of T_h by

$$a = -1.81674 \times 10^{-8}T_h{}^4 + 7.49047 \times 10^{-6}T_h{}^3 - 9.20595 \times 10^{-4}T_h{}^2 + 6.52266 \times 10^{-2}T_h - 9.89904 \times 10^{-1}$$

$$b = 7.56250 \times 10^{-6}T_h{}^2 - 4.45141 \times 10^{-3}T_h - 4.12191 \times 10^{-1}$$

According to Eq. (4), the C_{7+} mole percent depends uniquely on the determination of T_h and F_v of a petroleum inclusion. It is known that the molecular weight, density, and relative distribution of components (or lumped component fractions) in the C_{7+} fraction are expected to be very different in different types of reservoir fluids, e.g., gas condensates, volatile oils, black oils or heavy oils. The volumetric behavior of the C_{7+} fraction is sensitive to variations in the fluid type, as shown in Fig. 7. There is no obvious effect of the C_{7+} mole percent on F_v when the oils range from black oil to heavy oils, but there is a strong effect on F_v when the oils range from volatile oils to gas condensates. Table 6 shows the range of input variables used to develop the empirical correlation (Eq. (4)) for estimating the C_{7+} mole percent in an inclusion. Table 6 clearly shows that the correlation has been developed over a methane content range of 0.66–74.30% and a heptane plus fraction range of 9.82–83.99%, representing the full range of possible petroleum fluids from gas condensates to heavy oils except wet gas and dry gas. As composition data are unavailable for the source rock, we cannot ensure that the correlation actually holds over the entire range of possible fluid compositions for all source rock types. However, we believe that the correlation can be used for the petroleum fluids from different types of source rock because the reservoir fluids used in this study originate from all over the word and therefore cannot all be generated from the same source rock type.

However, F_v and T_h combined with the α–β model are not sufficient to constrain the petroleum inclusion composition [4,5]. Because of the problem of composition uncertainty, there is

Table 6
Range of input variables used in deriving the correlations between C_{7+} mole percent and F_v and T_h.

	Data used to develop the model		
	Min.	Ave.	Max.
N_2	0.00	0.47	3.92
CO_2	0.00	1.25	8.82
H_2S	0.00	0.17	4.78
C_1	0.66	37.17	74.30
C_2	0.58	7.65	14.09
C_3	0.41	6.27	10.51
C_4	0.92	4.42	8.42
C_5	0.39	3.13	6.67
C_6	0.00	2.92	6.68
C_{7+}	9.82	36.70	83.99
Temp. (°C)	43.35	89.26	156.67
P_s (MPa)	0.55	18.98	42.86

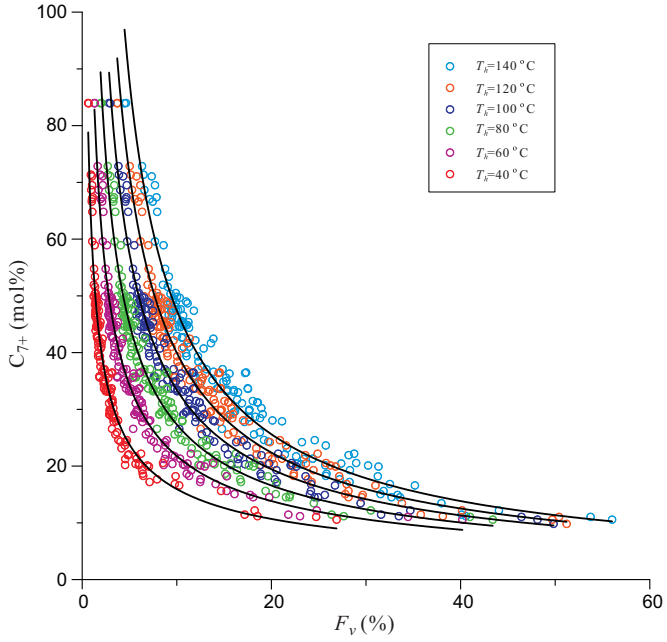

Fig. 7. Linear regression of the mole percent of C_{7+} cut of the adjusted experimental fluid [19,38,41–61] as a function of the degree of bubble filling, F_v (calculated at 20 °C) for various values of the homogenization temperature, T_h, using the volume calibration method.

nounique solution for a given T_h and F_v, which can be measured individually on one petroleum inclusion, and the full set of solutions is represented by an α–β curve [4,5]. One problem is that the α–β composition modeling is strongly affected by the calculated F_v using the *EOS*, and this modeling is used to fit the measured F_v. The uncertainties in the calculated F_v, modeled α–β curve, modeled composition and prediction of the saturation pressure are given in Tables 5 and 6 and Fig. 6. How can the effects of the modeled F_v on the α–β composition modeling be overcome? This problem can be solved using the direct link between the C_{7+} mole content and T_h and F_v provided by Eq. (4). The α–β solutions for a given T_h and F_v should correspond to the same C_{7+} mole content; otherwise, the modeled α–β curve will intersect the iso-C_{7+} curve (Eq. (4)) and a unique α–β value will be determined by the intersection of the α–β curve and iso-C_{7+} curve, which is inconsistent with the equilibrium thermodynamical conclusion that the T_h and F_v data are insufficient to determine the unique α–β parameters. For this reason, we first calculate the C_{7+} mole percent using Eq. (4) for a measured set of T_h and F_v values for a petroleum inclusion, and then compute the α–β curve with the identical C_{7+} mole percent using the α–β composition model. This simplified α–β modeling not only eliminates the effects of the calculated F_v using the *EOS* but also renders the method consistent with equilibrium thermodynamics. The α–β solutions for a petroleum inclusion with a given T_h, F_v, and hypothesized compositional distribution (α–β) can therefore be characterized simply by tuning the heptane plus mole fraction. The α–β parameters for the inclusion can then be determined by comparison to the α–β behavior of the natural oils or physical and chemical characteristics of the inclusion, e.g., the API degree and C_1 mole percent.

3.5. Constraining the trapping pressure prediction with the C_1 mole content

The determination of the trapping pressure requires T_h, F_v and the trapping temperature, T_t, of the petroleum inclusion. The measured T_h and F_v are usually coupled with an α–β composition model [4,5] or fluid model [3] and used to constrain the possible composition of the trapped petroleum by matching the calculated T_h and F_v. For the α–β model, the T_h and F_v values are not sufficient to determine the α–β parameters unambiguously: a wide range of α–β values can satisfy a given set of T_h and F_v data [4,5]. Additional parameters must therefore be used to delimit the range of probable values, e.g., the GOR, API degree or methane mole content [5]. Once the fluid composition is determined, the isochore in the single phase domain connecting the homogenization condition (e.g., the point (T_h, P_h) in Fig. 1) to the trapping condition (e.g., point (T_t, P_t) in Fig. 1) can be constructed, and the trapping pressure is easy to obtain if T_t is known. As stated earlier, the prediction of the trapping pressure is directly related to the saturation pressure and modeled petroleum composition, which is heavily impacted by inaccuracies in the calculation of F_v. However, for a given petroleum fluid whose fluid composition, physico-chemical characteristics (e.g., *MW* and *SG*) of the plus fraction and experimental saturation pressure are known, it is straightforward to obtain a reliable prediction of the saturation pressure and volume characteristics using the method in this paper. The trapping pressure can then be reliably reconstructed. This point is stressed in this study because a reliable trapping condition cannot be reproduced by experimental simulations (synthetic fluid inclusions), owing primarily to the difficulty of fixing the experimental petroleum composition, e.g., only dead oil was used in the synthetic petroleum inclusion experiment. However, a reliable prediction of the trapping pressure can be performed using the thermodynamic model presented in this study, potentially enabling the natural relations that appear to exist between P_t, T_h, and C_{7+}in petroleum inclusions to be deciphered.

The 160 petroleum fluids [19,38,41–61] are used as reference fluids, and the approximate saturation pressure, P_s, is computed artificially assuming various T_h values (T_h = 60 °C, 80 °C, 100 °C, 120 °C and 140 °C) after matching the saturation pressures of the reference oils using the method in this study (Appendix A). The calculated saturation pressures are regarded as the most reliable approximations to the true value. Ping et al. [12] has shown that the saturation pressure is a function of the C_1 mole percent. Fig. 8 shows the close agreement between the calculated saturation pressures and C_1 mole percent, as the saturation pressure is also related to T_h. We obtain the mathematical correlation between T_h and the C_1 mole percent using multi linear regression as follows:

$$P_h = aC_1{}^2 + bC_1 + c \tag{5}$$

where a, b and c are the coefficients, given as functions of T_h by

$$a = (a_1T_h{}^4 + a_2T_h{}^3 + a_3T_h{}^2 + a_4T_h + a_5) \times 10^{-4} \tag{6}$$

$$b = (b_1T_h{}^4 + b_2T_h{}^3 + b_3T_h{}^2 + b_4T_h + b_5) \times 10^{-2} \tag{7}$$

$$c = c_1T_h{}^4 + c_2T_h{}^3 + c_3T_h{}^2 + c_4T_h + c_5 \tag{8}$$

where the constant coefficients in Eq. (6) through Eq. (8) are given by:

$$a_1 = -1.31 \times 10^{-7};\ a_2 = 4.99 \times 10^{-5};\ a_3 = -8.31 \times 10^{-3};\ a_4 = 6.72 \times 10^{-1};\ a_5 = 20.30;$$
$$b_1 = 4.14 \times 10^{-8};\ b_2 = -1.56 \times 10^{-5};\ b_3 = 2.17 \times 10^{-3};\ b_4 = 2.88 \times 10^{-2};\ b_5 = 18.70;$$
$$c_1 = -9.18 \times 10^{-9};\ c_2 = 3.42 \times 10^{-7};\ c_3 = -6.60 \times 10^{-5};\ c_4 = 1.39 \times 10^{-2};\ c_5 = 4.28 \times 10^{-1}.$$

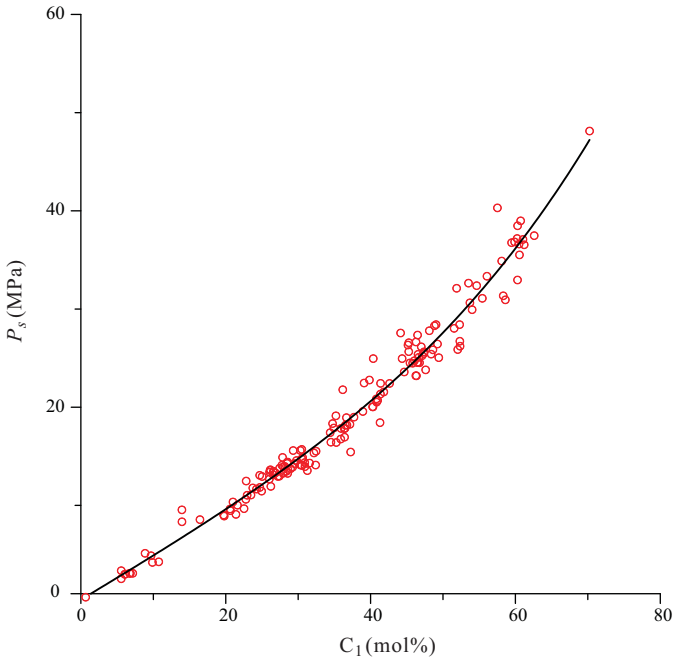

Fig. 8. Regression curve of the calculated saturation pressure (P_s) (T_h = 100 °C) as a function of the adjusted experimental C_1 mole percent of the reservoir fluids [19,38,41–61].

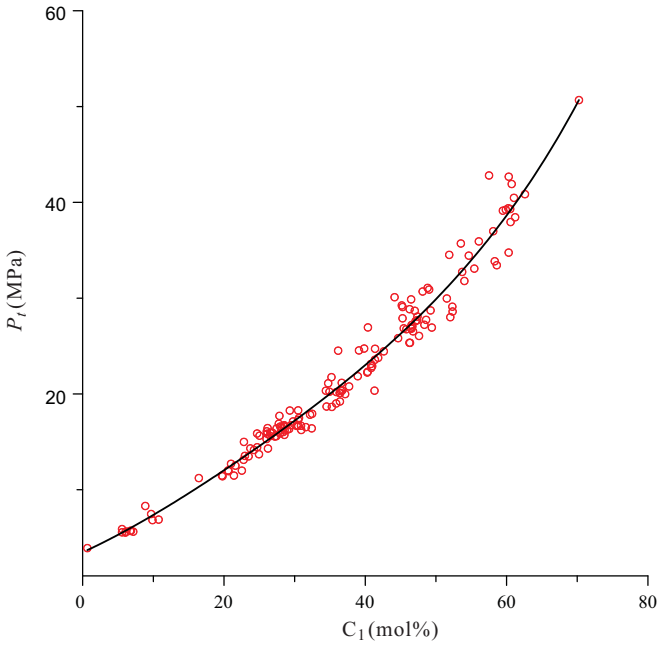

Fig. 9. Regression curves of the calculated trapping pressure (P_t) (T_h = 100 °C, T_t = 105 °C) as a function of the adjusted experimental C_1 mole percent of the reservoir fluids [19,38,41–61].

The accuracy of Eq. (5) is tested below. The calculated pressures are compared with the experimental values, and an *AAD*% of 7.20 is obtained (Table 7). The method of Eq. (5) is also compared to the relationship given in Elsharkawy [19], which was obtained using multilinear regression on the petroleum composition (N_2, CO_2, H_2S, and C_1 to C_{7+}) and *MW* and *SG* of the heptane plus fraction. Table 7 shows that Eq. (5) is slightly superior to the empirical relation, but note that the former uses only one independent parameter, x_1, in place of the twelve input variables used in Elsharkawy [19]. Eq. (5) therefore appears to be more suitable for application to petroleum inclusions given the difficulty of obtaining the detailed composition and physical parameters of the petroleum.

The strong correlation between the saturation pressure and C_1 mole percent motivated us to seek a relationship between the trapping pressure, P_t, and the C_1 mole percent. Several sets of P_t and C_1 mole percent data were used to fit the correlation between them, and Fig. 9 shows the tight relationship between P_t (T_h = 100 °C, T_t = 105 °C) and the C_1 mole percent. In addition, we found that the fit becomes gradually worse with increasing discrepancy between T_t and T_h. The fitted correlation between the trapping pressure, P_{T_h+5} ($T_t = T_h + 5$ °C), and the C_1 mole percent is given by

$$P_{T_h+5} = aC_1{}^2 + bC_1 + c \tag{9}$$

where a, b and c are the coefficients, given as a function of T_h by

$$a = (a_1T_h{}^4 + a_2T_h{}^3 + a_3T_h{}^2 + a_4T_h + a_5) \times 10^{-4} \tag{10}$$

$$b = (b_1T_h{}^4 + b_2T_h{}^3 + b_3T_h{}^2 + b_4T_h + b_5) \times 10^{-2} \tag{11}$$

$$c = c_1T_h^4 + c_2T_h^3 + c_3T_h^2 + c_4T_h + c5. \tag{12}$$

The constant coefficients in Eq. (10) through Eq. (12) are given by

$$a_1 = -1.56 \times 10^{-7};\ a_2 = 5.72 \times 10^{-5};\ a_3 = 9.06 \times 10^{-3};\ a_4 = 7.09 \times 10^{-1};\ a_5 = 19.70$$
$$b_1 = 5.25 \times 10^{-8};\ b_2 = -1.91 \times 10^{-5};\ b_3 = 2.55 \times 10^{-3};\ b_4 = 1.43 \times 10^{-2};\ b_5 = 17.00$$
$$c_1 = -1.98 \times 10^{-9};\ c_2 = 6.60 \times 10^{-7};\ c_3 = -6.46 \times 10^{-5};\ c_4 = -5.23 \times 10^{-3};\ c_5 = 5.05.$$

The trapping condition (T_h + 5, P_{T_h+5}) and homogenization conditions (T_h, P_h or P_s) of the petroleum inclusion were correlated with the only unknown parameter, the C_1 mole percent. The slope of the isochore, k(dP/dT), which connects the trapping condition to the homogenization conditions can be determined by the two points (T_h + 5, P_{T_h+5}) and (T_h, P_h or P_s) in the P–T phase diagram (Fig. 1b). The slope is given by

$$k = \frac{P_{T_h+5} - P_h}{5}. \tag{13}$$

The isochore slope, k, is also a function of the C_1 mol% according to Eqs. (5) and (9). We can therefore intuitively calculate an isochore for a petroleum inclusion and then incorporate other pieces of data to help constrain P_t and T_t (e.g., the homogenization temperature of the coexisting aqueous, thermobaric gradient from a basin model). The trapping pressure, P_t, at any T_t on the isochore is then calculated as

$$P_t = P_h + k(T_t - T_h) \tag{14}$$

where P_h is given by Eq. (5) and k is given by Eq. (13).

Eq. (14), which is a function of only one independent variable (C_1 mol%), is very attractive because the trapping pressure

Table 7
Comparison of the predicted saturation pressures using the method in this study (Eq. (5)) and the empirical correlation.

Method	*ARD* (*P*)%	*AAD* (*P*)%
Eq. (5)	2.33	7.20
Empirical model[a]	−2.59	9.23

[a] Elsharkawy (2003) [19].

Table 8
Strategies for trapping pressure prediction and prediction comparison.

Strategies	Input parameters	Procedure parameters	ΔT_h (10 °C)		ΔT_h (20 °C)		ΔT_h (30 °C)		ΔT_h (40 °C)		ΔT_h (50 °C)		*ARD* (P_t)	*AAD* (P_t)
			ARD (P_t)	*AAD* (P_t)	*ARD* (P_t)	*AAD* (P_t)	*ARD* (P_t)	*AAD* (P_t)	*ARD* (P_t)	*AAD* (P_t)	*ARD* (P_t)	*AAD* (P_t)		
1	C_1, T_h, ^1T_t	^4P_h, $^5P_{T_h+5}$	0.83	5.85	1.21	5.92	1.59	6.09	2.47	6.43	2.94	6.73	2.13	6.44
2	C_1, T_h, F_v, ^2T_t	$^1C_{7+}$, $^2\alpha$-β, ^1P_s	−6.28	8.49	−5.20	7.23	−4.46	6.53	−3.91	5.82	−3.49	5.51	−4.85	6.92
3	T_h, F_v, ^1T_t	$^1C_{7+}$, $^3C_1$, ^4P_h, $^5P_{T_h+5}$	−1.59	16.18	−0.85	13.86	−0.27	12.33	1.41	10.96	2.07	10.37	0.28	13.07
4	T_h, F_v, ^2T_t	$^1C_{7+}$, $^3C_1$, $^2\alpha-\beta$, ^1P_s	−9.27	18.06	−7.84	15.47	−6.98	13.78	−5.30	11.86	−4.71	11.04	−7.17	14.54

ΔT_h, means the difference between the trapping temperature, T_t and the homogenization temperature, T_h; *ARD*, average relative deviation; *AAD*, average absolute deviation; P_t means the trapping pressure at the trapping temperature, T_t; P_{T_h+5} means the trapping pressure at the trapping temperature, $T_h + 5$ °C; P_h means homogenization pressure at the homogenization temperature (T_h); ^1P_s means the saturation pressure of α–β composition, which is calculated by the method 1 in Table 1; $^1C_{7+}$ means the mole content of C_{7+} fraction is from Eq. (4) in this paper; $^2\alpha$–β means the α–β composition is obtained from the simplified α–β modeling in this paper; $^3C_1$ means the mole content of C_1 fraction is from the empirical correlation [12]; ^4P_h means the P_h is obtained from Eq. (5); $^5P_{T_h+5}$ means the P_{T_h+5} is obtained from Eq. (9); ^1T_t means trapping pressure is obtained from the Eq. (14); ^2T_t means trapping pressure is obtained from the thermodynamics calculation by *EOS* based on the determined α–β composition.

estimation is usually performed through a series of complex *PVT* thermodynamic calculations, which are often assisted by professional software [3–5]. More importantly, Eq. (14) is independent of F_v and is therefore immune to the effects of F_v on the composition modeling. However, we cannot verify the accuracy of the trapping pressure prediction with data acquired on natural or synthetic inclusions using Eq. (14) because the detailed compositions of natural or synthetic petroleum inclusions cannot be determined precisely, especially for the C_1 mol%. In addition, we do not know the exact trapping pressure of the fluid inclusion even for the synthetic inclusions. To back-check the methods of trapping pressure predictions in this paper, we use the tuned *EOS* with the volume correction to iteratively calculate several *P*–*T* points (P_{rt}–T_{rt}) at equal density along an isochore for a given fluid of known composition, and observe how well the empirical correlation to C_1 mol% (Eq. (14)) is matched. We compare the P_{rt} with the calculated values using the empirical correlation of Eq. (14) and the simplified thermodynamic method (Eq. (4)). As stated previously, Eq. (4) is not sufficient to determine the α–β parameters unambiguously, and the mole content of C_1 has therefore been used to determine the approximate petroleum inclusion composition. Both the calculated C_1 mole content (obtained from the C_{7+} mole percent [12]) and the

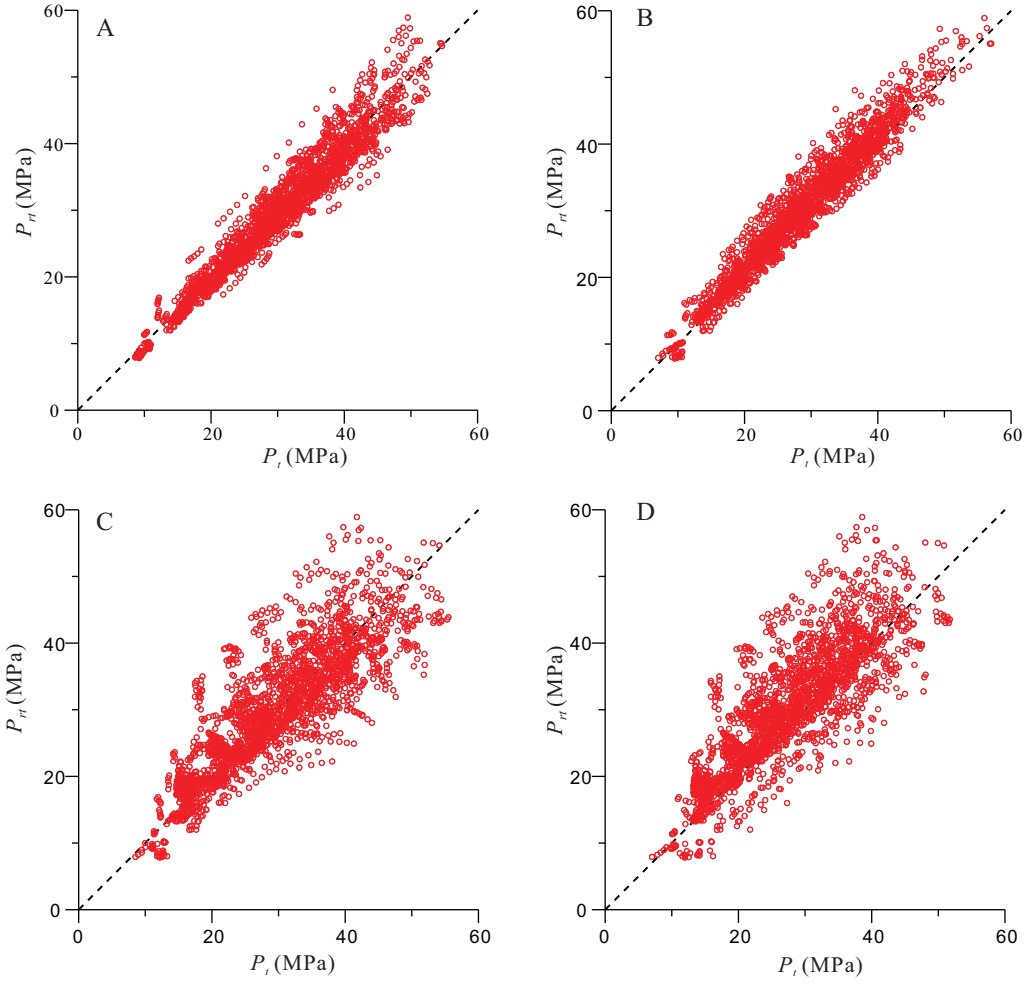

Fig. 10. Comparison of the reference trapping pressure (P_{rt}) of the adjusted experimental fluids [19,38,41–61] with the calculated values using the various strategies in Table 8. The trapping pressures were calculated at various homogenization temperatures (T_h = 60 °C, 80 °C, 100 °C, 120 °C) with trapping temperatures ($T_t = T_h + 10$ °C, $T_h + 20$ °C, $T_h + 30$ °C, $T_h + 40$ °C, $T_h + 50$ °C), respectively.

true C_1 mole content have been used to constrain Eq. (14) and the α–β composition once the $\beta(\alpha)$ curve is obtained using Eq. (4) and the α–β model. There are therefore four strategies for predicting the trapping pressure, using the methods of Eqs. (4) and (14) and the two constraining conditions (true C_1 mol content and calculated value based on the Ping et al. correlation [12]), which are shown in Table 8 along with the comparison results at different ΔT_h (10–50 °C) values. The predictions of the four strategies for the trapping pressure are given in Fig. 10.

As shown in Table 8, both methods provide a better prediction of P_t under various trapping conditions (ΔT_h: 10–50 °C) when the true C_1 mole content of the petroleum inclusion is known (strategy 1 and strategy 2); however, strategies 3 and 4 have errors twice as large as strategies 1 and 2 because the C_1 mole content of the petroleum inclusion is not the true value but that calculated using the correlation of Ping et al. [12]. Fig. 10 clearly indicates that the accuracy of the trapping pressure prediction is improved greatly if the mole content of C_1 has been determined accurately. These results are also in accordance with the statement that the best constraining parameter for the pressure modeling is the methane mole fraction [12]. The choice of strategy depends on the objective of the users and available data. Strategy 1 is the best method to obtain the trapping pressure if the mole content of C_1 is available, and strategy 2 is the best method to obtain the α–β composition if the mole content of C_1 is available. Note that the input F_v and saturation pressure prediction in strategy 2 can increase the uncertainty for determining the α–β composition and trapping condition, which depend on the accuracy of the measured F_v in the laboratory and the correlations used to estimate the saturation pressure. When the mole content of C_1 is not available, the F_v and T_h values of the petroleum inclusion are used to calculate the C_{7+} mole content, and the mole content of C_1 can be calculated from the correlation of Ping et al. [12]. In this case, we cannot obtain a significantly more accurate trapping pressure prediction than that obtained using strategy 3 or 4.

4. Conclusions

In this paper, a method has been proposed to improve the accuracy of the volume and saturation pressure determinations of petroleum fluids to predict the trapping pressure in petroleum inclusions. Using a compilation of 160 measured composition and saturation pressure data and 909 relative volume data (N = 397 (*CME*), N = 71 (*DV*), N = 441 (*SWT*)) from the literature, we show that the method in this paper is able to predict the volume characteristics and F_v of the petroleum inclusion.

The F_v parameter is important in addition to the saturation pressure because of its effect on the composition modeling and estimation of the petroleum trapping pressure. As F_v is a good indicator of the C_{7+} fraction (Fig. 10), it is possible to simplify the thermodynamical modeling of the petroleum in an α–β composition model by tuning the mole content of C_{7+} to match the calculated value based only on its microthermometric signature (T_h, F_v) (Eq. (4)). The simplified method overcomes the deviation caused by the calculation of F_v from the *EOS* and is easier to use.

This study also provides evidence of the influence of the bulk methane content on the homogenization pressure, P_h, as illustrated in Fig. 8 and Eq. (5). Furthermore, the trapping pressure P_{T_h+5} ($T_t = T_h + 5$) is also correlated with the bulk methane content of the petroleum inclusion (Eq. (9)). Thus far, the trapping pressure, P_t, at a given trapping temperature, T_t, can only be calculated using Eq. (14), which is a function of the bulk methane content and T_h of the petroleum inclusion. The bulk methane content can be measured using FT-IR spectroscopy [63] or three-dimensional multi modal coherent anti-Stokes Raman scattering (CARS) microscopy [64]. We have evaluated the effects of varying the bulk methane content on the estimation of the trapping pressure for both the new composition modeling method (Eq. (4)) and the correlation given by Eq. (14). We conclude that the methane mole fraction plays an important role in the trapping pressure prediction, and future research efforts should focus on this observation.

List of symbols

T	temperature (°C)
P	pressure (MPa)
T_h	homogenization temperature (°C)
P_h	homogenization pressure (MPa)
F_v	bubble filling fraction (%)
T_v	measurement temperature of F_v (°C)
P_v	pressure at T_v (MPa)
P_t	trapping pressure (MPa)
P_{T_h+5}	trapping pressure at (T_h + 5) °C (MPa)
P_{rt}	reference trapping pressure (MPa)
P_s	saturation pressure (MPa)
T_t	trapping temperature (°C)
k	isochore slope
α, β	parameters of the α–β model
n	number of carbon atoms
C_1	methane
x_i	mole fraction of component (or pseudo-component) i
MW	molar weight (g/mol)
SG	specific gravity
ARD	average relative deviation (%)
AAD	average absolute deviation (%)
Δx	absolute deviation between the experimental and tuned compositions
exp	experimental
tun	tuned
calc	calculated
N	number of data points
T_c	critical temperature (K)
P_c	critical pressure (bar)
ω	acentric factor
T_b	boiling temperature (K)
k_{ij}	binary interaction parameter
Min.	minimum
Ave.	average
Max.	maximum
Temp.	temperature
CME	constant mass expansion
DV	isothermal differential vaporization
SWT	isothermal swelling test

Acknowledgements

This paper was jointly funded by China's 973 National Key Research and Development Program (Grant No. 2012CB214804) and the National Natural Science Foundation of China (NSFC) (Grant No. 41202088), and the Fundamental Research Funds for the Central Universities, China University of Geosciences (Wuhan) (Grant No. cug130104).

Appendix A. A method for matching the saturation pressures of petroleum fluids

The following rationale was followed to match the saturation pressure by adjusting the *MW* and density of the heptane plus

fraction. First, the apparent *MW* of the petroleum fluid is calculated with the following equation:

$$M_a = \sum_{i=1}^{n} Z_i MW_i \tag{A.1}$$

Then, the weight fraction of each component in the fluid is determined using the reported mole fractions.

$$W_i = \frac{Z_i MW_i}{M_a} \tag{A.2}$$

During adjusting, the weight fractions are maintained constant, and the molar composition is recalculated with each change in the *MW* of the heptane plus fraction. It is more convenient to modify the apparent *MW* of the fluid because this has the same effect as modifying the *MW* of the plus fraction [21].

After adjustment of the apparent *MW* of the fluid, the new molar composition of all components except the heptane plus fraction is calculated as follows:

$$Z_i = \frac{W_i M_a}{MW_i} \tag{A.3}$$

then the mole fraction of the heptane plus fraction is calculated.

$$Z_{plus} = 1 - \sum_{i=1}^{n-1} Z_i \tag{A.4}$$

the *MW* of the plus fraction is recalculated as follows:

$$MW_{plus} = \frac{M_a - \sum_{t=1}^{n-1} Z_i MW_i}{Z_{plus}} \tag{A.5}$$

and the density of the plus fraction is then calculated.

$$\rho_{plus} = \frac{Z_{plus} MW_{plus} \rho^*_{plus}}{Z^*_{plus} MW^*_{plus}} \tag{A.6}$$

where Z^*_{plus} MW^*_{plus} and ρ^*_{plus} are reported mole fraction, *MW* and density of the plus fraction. Z_{plus} MW_{plus} and ρ_{plus} are adjusted mole fraction, *MW* and density of the plus fraction.

Appendix B. A method for volume calibration of petroleum fluids

Several volumetric experiments are typically used to verify the equation of state (*EOS*), for example, the isothermal constant massexpansion (*CME*), isothermal differential vaporization (*DV*) and isothermal swelling test (*SWT*). The constant massexpansion experiment is usually conducted to determine the bubble point pressure at a selected temperature. The principle of the experiment has been described in detail by Pedersen et al. [33]. The constant massexpansion experiment provides information on the relative volumetric amounts of gas and liquid at a specified temperature at various pressures. The relative volume is defined as:

$$V_t^{rel} = \frac{V_t^P}{V_t^{ps}} \tag{B.1}$$

where V_t^P is the total volume at pressure P and temperature t, V_t^p is the total volume at bubble point pressure P_s and temperature t and V_t^{rel} is the relative volume at pressure P and temperature t. V_t^p is given by:

$$V_t^P = V_G^P + V_L^P \tag{B.2}$$

where V_G^P is the volume of the gas phase at pressure P and temperature t and V_L^P is the volume of the liquid phase at the same pressure and temperature as V_G^P.

Combining Eqs. (B.2) and (B.1) gives

$$V_t^{rel} = \frac{V_t^P}{V_t^{ps}} = \frac{V_G^P + V_L^P}{V_t^{ps}} \tag{B.3}$$

The F_v value at pressure P and temperature t is defined as:

$$F_v = \frac{V_G^P}{V_G^P + V_L^P} \tag{B.4}$$

Substituting Eqs. (B.2) and (B.4) into (B.1) gives

$$V_t^{rel} = \frac{V_t^P}{V_t^{ps}} = \frac{(V_G^P + V_L^P)}{V_t^{ps}} = \frac{V_L^P}{(1 - F_V) V_t^{ps}} \tag{B.5}$$

Eq. (B.5) can be rearranged to allow direct calculation of the F_v as follows:

$$F_v = 1 - \frac{V_L^P}{V_t^{rel} V_t^{ps}} = 1 - \frac{V_t^{rel'}}{V_t^{rel}} \tag{B.6}$$

where $V_t^{rel'}$ is the relative volume of the liquid phase, given by:

$$V_t^{rel'} = \frac{V_L^P}{V_t^{ps}} \tag{B.7}$$

Eq. (B.6) shows that F_v is function of V_t^{rel} and $V_t^{rel'}$. Clearly, improvement upon the calculation of F_v can be achieved indirectly by making an accurate prediction of both V_t^{rel} and $V_t^{rel'}$. The *SWT* experiment is usually used to evaluate the volume effect of the swelling of the oil when gas is injected into a reservoir containing an under saturated oil. After a predetermined amount of gas is introduced into the under saturated oil, a *CME* experiment is performed to determine the saturation pressure and relative volume (V_t^{rel}) of the new mixture, where the relative volume is defined to be the same as V_t^{rel} in the *CME* experiment. The relative volume in the *DV* experiment is defined as V_{liq}/V_{sat}, similar to the definition of $V_t^{rel'}$ in Eq. (B.7), where V_{liq} is the liquid phase volume at pressure P and V_{sat} is the liquid volume at the bubble pressure. Therefore, both the *SWT* and *CME* experiments can provide the V_t^{rel} information for the oils, and the *IDV* experiment can provide the $V_t^{rel'}$ information.

The relative volume (V_t^{rel} and $V_t^{rel'}$) data have been matched using volume translation [65]. Péneloux et al. [65] demonstrated that the introduction of a volume shift parameter in cubic equations of state, such as the *PR-EOS*, does not affect the vapor–liquid equilibrium calculations and therefore does not affect the original gas–liquid equilibrium capacity of the equation of state. The volume translation parameters are correction terms that are applied to molar volume calculated from the *PR-EOS*:

$$V_L = V_L^{EOS} - \sum_{i=1}^{m} x_i c_i \tag{B.8}$$

$$V_G = V_G^{EOS} - \sum_{i=1}^{m} y_i c_i \tag{B.9}$$

where V_L^{EOS} and V_G^{EOS} are the liquid and gas molar volumes calculated from the *EOS*, and c_i is the molar volume translation parameter for component i.

Jhaveri and Youngren [51] defined a dimensionless shift parameter by dividing the volume translation parameter, c, by the second *PR-EOS* parameter, b. These two parameters have the same units of molar volume. A dimensionless parameter is therefore defined as follows:

$$S_i = \frac{c_i}{b_i} \tag{B.10}$$

where b_i is the equation of state constant, given by:

$$b_i = 0.0778\frac{RT_{ci}}{P_{ci}} \tag{B.11}$$

For pure compositions, the volume shift parameters can be found in Jhaveri and Youngren [51], and the volume shift parameters for pseudocomponents C_{n1} and C_{n2} were calculated using a simple correlation:

$$S = 1 - \frac{d}{MW^e} \tag{B.12}$$

The values of coefficients d and e are used as regression variables to match the *CME*, *DV*, and *SWT* data (V_t^{rel} and $V_t^{rel'}$).

References

[1] E. Roedder, Mineralogical Society of America, Washington, 1984.
[2] R.H. Goldstein, T.J. Reynolds, Society of Sedimentary Geology (SEPM), Tulsa, 1994.
[3] A.C. Aplin, G. Macleod, S.R. Larter, K.S. Pedersen, H. Sorensen, T. Booth, Mar. Petrol. Geol. 16 (1999) 97–110.
[4] R. Thiéry, J. Pironon, F. Walgenwitz, F. Montel, J. Geochem. Explor. 69–70 (2000) 701–704.
[5] R. Thiéry, J. Pironon, F. Walgenwitz, F. Montel, Mar. Petrol. Geol. 19 (2002) 847–859.
[6] H.-Y. Tseng, R.J. Pottorf, Mar. Petrol. Geol. 19 (2002) 797–809.
[7] I.A. Munz, M. Wangen, J.-P. Girard, J.-C. Lacharpagne, H. Johansen, Mar. Petrol. Geol. 21 (2004) 1043–1060.
[8] J. Pironon, Acta Petrol. Sin. 20 (2004) 1333–1342.
[9] J. Bourdet, J. Pironon, G. Levresse, J. Tritlla, Geofluids 8 (2008) 46–59.
[10] J. Pironon, J. Bourdet, Geochim. Cosmochim. Acta 72 (2008) 4916–4928.
[11] J. Bourdet, J. Pironon, G. Levresse, J. Tritlla, Mar. Petrol. Geol. 27 (2010) 126–142.
[12] H. Ping, R. Thiéry, H. Chen, Geofluids 11 (2011) 328–340.
[13] F. Montel, Fluid Phase Equilibr. 84 (1993) 343–367.
[14] I.A. Munz, H. Johansen, I. Johanse, SPE Annual Technical Conference and Exhibition, SPE, Houston, TX, 1999, p. 56519-MS.
[15] C.R. Evans, M.A. Rogers, N.J.L. Bailey, Chem. Geol. 8 (1971) 147–170.
[16] P. Blanc, J. Connan, AAPG Memoir. 60 (1994) 237.
[17] J. Pironon, M. Canals, J. Dubessy, F. Walgenwitz, C. Laplace-Builhe, Eur. J. Miner. 10 (1998) 1143–1150.
[18] J.-N. Jaubert, L. Avaullee, J.-F. Souvay, J. Petrol. Sci. Eng. 34 (2002) 65–107.
[19] A.M. Elsharkawy, J. Petrol. Sci. Eng. 38 (2003) 57–77.
[20] P. Thomassen, K.S. Pedersen, A. Fredenslund, SPE, 1987, 16036-MS.
[21] R.A.A. Zurita, J. William, D. McCain, SPE Annual Technical Conference and Exhibition, SPE, San Antonio, TX, 2002, p. 77382.
[22] A.A. Al-Meshari, S. Armco, W.D. MaCain, SPE Middle East Oil and Gas Show and Conference, SPE, Kingdom of Bahrain, 2007, p. 104631.
[23] D. Peng, D. Robinson, Ind. Eng. Chem. Fundam. 15 (1976) 59–64.
[24] T. Ahmed, G. Cady, A. Story, SPE Annual Technical Conference and Exhibition, SPE, Las Vegas, Nevada, 1985, p. 14266-MS.
[25] D. Katz, A. Firoozabadi, J. Petrol. Technol. 30 (1978) 1649–1655.
[26] R. Cavett, Proc. 27th Annual Meeting, American Petroleum Institute, Dallas, 1962, pp. 351–366.
[27] M.R. Riazi, T.A. Al-Sahhaf, Fluid Phase Equilibr. 117 (1996) 217–224.
[28] W.C. Edminster, Pet. Refiner. 37 (1958) 173–179.
[29] F. Winn, Pet. Refiner 36 (1957) 157–159.
[30] M.G. Kesler, B.I. Lee, Hydrocarbon Process. 55 (1976) 153–158.
[31] M. Riazi, T. Daubert, Hydrocarbon Process. 59 (1980) 115–116.
[32] C.H. Twu, Fluid Phase Equilibr. 16 (1984) 137–150.
[33] K. Pedersen, A. Fredenslund, P. Thomassen, Contributions in Petroleum Geology & Engineering, Gulf Pub. Co., Houston, 1989, p. 252.
[34] L. Avaullee, L. Trassy, E. Neau, J.N. Jaubert, Fluid Phase Equilibr. 139 (1997) 155–170.
[35] T. Hantschel, A.I. Kauerauf, Fundamentals of Basin and Petroleum Systems Modeling, Springer, 2009.
[36] K.S. Pedersen, P. Rasmussen, A. Fredenslund, Ind. Eng. Chem. Proc. Des. Dev. 24 (1985) 948–954.
[37] C. Whitson, Soc. Pet. Eng. J. 24 (1984) 685–696.
[38] T. Ahmed, Hydrocarbon Phase Behavior, Gulf Pub. Co., Houston, 1989.
[39] J.-N. Jaubert, F. Mutelet, Fluid Phase Equilibr. 224 (2004) 285–304.
[40] J.-N. Jaubert, R. Privat, F. Mutelet, AIChE J. 56 (2010) 3225–3235.
[41] R. Agarwal, Y. Li, L. Nghiem, SPE Reservoir Eng. 5 (1990) 115–120.
[42] A. Al-Meshari, Petroleum Engineering, Texas A&M University, 2004248.
[43] L. Avaullee, E. Neau, J.-N. Jaubert, Fluid Phase Equilibr. 139 (1997) 171–203.
[44] K. Coats, G. Smart, SPE Reservoir Eng. 1 (1986) 277–299.
[45] A. Danesh, D. Xu, A. Todd, SPE Reservoir Eng. 7 (1992) 343–348.
[46] A. Hoffman, J. Crump, C. Hocott, Trans. Am. Inst. Mining Metall. Petrol. Eng. 198 (1953) 1–10.
[47] K. Hong, SPE Enhanced Oil Recovery Symposium, SPE, Tulsa, Oklahoma, 1982, p. 10691-MS.
[48] R.H. Jacopy, V.J. Berry, Petrol. Trans. Trans. Am. Inst. Mining Metall. Petrol. Eng. 213 (1958) 59–65.
[49] J.-N. Jaubert, E. Neau, L. Avaullee, G. Zaborowski, Ind. Eng. Chem. Res. 34 (1995) 4016–4032.
[50] J.-N. Jaubert, E. Neau, A. Peneloux, C. Fressigne, A. Fuchs, Ind. Eng. Chem. Res. 34 (2002) 640–655.
[51] B. Jhaveri, G. Youngren, SPE Reservoir Eng. 3 (1988) 1033–1040.
[52] Y. Li, L. Nghiem, A. Siu, J. Can. Petrol. Technol. 24 (1985) 29–36.
[53] W.D. McCain, J. Petrol. Technol. 46 (1994) 746–750.
[54] H.M. Moharam, Ind. Eng. Chem. Res. 34 (1995) 4140–4144.
[55] E. Neau, J.N. Jaubert, M. Rogalski, Ind. Eng. Chem. Res. 32 (1993) 1196–1203.
[56] K. Pedersen, P. Thomassen, A. Fredenslund, Chem. Eng. Sci. 43 (1988) 269–278.
[57] K.S. Pedersen, A.L. Blilie, K.K. Meisingset, Ind. Eng. Chem. Res. 31 (1992) 1378–1384.
[58] L.S. Wang, J. Gmehling, AIChE J. 45 (1999) 1125–1134.
[59] C.A. Williams, E.N. Zana, G.E. Humphrys, SPE/DOE Enhanced Oil Recovery Symposium, Society of Petroleum Engineers, Tulsa, Oklahoma, 1980.
[60] R. Wu, L. Rosenegger, J. Can. Petrol. Technol. 38 (1999) 97–105.
[61] T. Yang, W.D. Chen, T.M. Guo, Fluid Phase Equilibr. 128 (1997) 183–197.
[62] D. William, J. McCain, The Properties of Petroleum Fluids, Pennwell Publishing Company, Tulsa, 1990.
[63] J. Pironon, R. Thiery, M. Ayt Ougougdal, S. Teinturier, G. Beaudoin, F. Walgenwitz, Geofluids 1 (2001) 2–10.
[64] R.C. Burruss, A.D. Slepkov, A.F. Pegoraro, A. Stolow, Geology 40 (2012) 1063–1066.
[65] A. Péneloux, E. Rauzy, R. Fréze, Fluid Phase Equilibr. 8 (1982) 7–23.